

Dalton Transactions

An international journal of inorganic chemistry

Accepted Manuscript

This article can be cited before page numbers have been issued, to do this please use: X. Zhang, L. Hongxiao, H. Chen and L. Fan, *Dalton Trans.*, 2020, DOI: 10.1039/D0DT02730H.



This is an Accepted Manuscript, which has been through the Royal Society of Chemistry peer review process and has been accepted for publication.

Accepted Manuscripts are published online shortly after acceptance, before technical editing, formatting and proof reading. Using this free service, authors can make their results available to the community, in citable form, before we publish the edited article. We will replace this Accepted Manuscript with the edited and formatted Advance Article as soon as it is available.

You can find more information about Accepted Manuscripts in the [Information for Authors](#).

Please note that technical editing may introduce minor changes to the text and/or graphics, which may alter content. The journal's standard [Terms & Conditions](#) and the [Ethical guidelines](#) still apply. In no event shall the Royal Society of Chemistry be held responsible for any errors or omissions in this Accepted Manuscript or any consequences arising from the use of any information it contains.

One Heterometallic {ZnEu}-Metal-Organic Framework for Efficient Chemical Fixation of CO₂

Hongxiao Lv, Hongtai Chen, Liming Fan and Xiutang Zhang*

Department of Chemistry, College of Science, North University of China, Taiyuan 030051, People's Republic of China. E-mail: xiutangzhang@163.com;

Received (in XXX, XXX) 1st January 2019, Revised Manuscript received 1st January 2019

Based on the ligand-directed synthetic strategy, the acidic solvothermal reaction of ZnO, Eu₂O₃, and 4,4',4''-(pyridine-2,4,6-triyl)tri(1,3-benzenedicarboxylic acid) (H₆PTTBA) generated one targeted robust double-walled honeycomb material of {[Eu^{III}Zn^{II}(HPTTBA)(H₂O)]·4DMF·3H₂O}_n (simplified as **NUC-9**), which featured the excellent characteristics of dual tubular nanochannels, high porosity and specific surface area, abundant exposed active metal sites, etc. Although both types of nano-channels (**I** and **II**) alternately arranged in the lattice and shaped by six rows of [Eu^{III}Zn^{II}(CO₂)₆(H₂O)] SBUs possessed the equal amount of exposed active metal sites, they could be differentiated according to the discrepant inner surface functionalized by free carboxyl oxygen atoms or coordinated aqueous molecules. Moreover, the activated sample of **NUC-9** exhibited the better catalytic performance than documented Zn- or Eu-based MOFs for the chemical transformation of various epoxides into the related carbonates under comparatively mild conditions of 1 atm CO₂ flow and 70 °C, which should be ascribed to that unsaturated ions of Zn²⁺ and Eu³⁺ as strong Lewis acid and free carboxyl oxygen atoms as basic sites could synergistically polarize and activate the substrates of epoxides and CO₂ and consequently prompt the reaction. Furthermore, the water-resistant framework of **NUC-9** could selectively and sensitively discriminate Fe³⁺ in aqueous solution according to fluorescence quenching effect. In addition, it's worth mentioning that the successful self-assembly of **NUC-9** provides one effective synthetic technique by employing designed favorable organic ligand for achieving the targeted functional model of MOFs.

Introduction

The warming of the Earth and the consequent climatic changes caused by greenhouse gases has become one of the greatest threats facing mankind today, such as sea level rise, land desertification, and extinction of some biological species.¹ Among all greenhouse gases (CO₂, N₂O, CH₄, etc), carbon dioxide accounts for the largest proportion and its concentration in the atmosphere has been steadily rising due to the persistently excessive consumption of fossil fuels in the areas of thermal power generation, industrialization, transportation vehicles, and so on. Therefore, the strategic research on the capture-storage or consumption of CO₂ in the atmosphere has become one urgent issue. At present, catalytic conversion of captured CO₂ into fuel or industrial raw materials is one of the most promotable ways to jointly solve the environmental and energy challenges.² Moreover, a series of research in recent years evidenced that porous metal-organic frameworks (MOFs) could be taken as effective heterogeneous catalysts for the chemical transformation of CO₂ and epoxides into carbonates and meantime was superior to homogeneous catalysts in the aspect of product separation and catalyst recycling.³ Furthermore, the mild reaction conditions of temperature and pressure by utilizing MOFs catalyst are incomparable with other hetero- or homogeneous catalysts, for instance, zeolites, inorganic metal salts or oxides, ionic liquids, amine aqueous solutions, polymerized organics, etc.⁴ Whereas, MOFs, as a kind of organic-inorganic hybrid material with marvellous structural adaptability, feature the excellent traits of high specific surface area and syngenetic micropore size, which consequently lead to the better unique adsorption performance for

CO₂.⁵ Thus, in order to promote the selective adsorption capacity of CO₂ in terms of kinetics and thermodynamics, the particular research interest for MOFs at present is concentrated on the performance optimization by designing functional organic ligands to adjust pore size, increasing the open metal sites to improve their adsorption affinity for CO₂, and improving the thermal and chemical stability (e.g. water resistance).⁶

Among all documented MOFs, zinc cation, as one kind of d-block metal ions and one potential strong Lewis acid, has been paid close attention due to its distinctive characteristics including electronic configuration, binding energy, and charge distribution, which renders it various coupling affinities to multifarious donor atoms from ligands.⁷ So far, quantum chemical calculation with ab initio calculations exhibited that the formation of hexa-coordinated Zn²⁺ cations was the most stable due to the largest binding energies, which could be confirmed by the absolute large proportion of Zn-MOFs constructed from hexa-coordinated Zn²⁺ ions.⁸ Whereas, recently reported Zn-MOFs based on tetra-coordinated Zn²⁺ ions with solvent-free channels could display the better selective adsorption performance for guest molecules of CO₂ and catalyze the chemical transformation of epoxides with CO₂ into according alkyl carbonates due to that exposed active Zn²⁺ ions as the strong Lewis acid to polarize and activate CO₂ and the ring of ethylene oxide *via* coordination affinity.⁹ So, the self-assembly of nanoporous Zn-MOFs with the purpose of enhancing the amount of exposed active tetra- or penta-coordinated Zn²⁺ cations will become a research hotspot, especially for the application in the areas of selectively separation or/and storage of guest molecules, catalysis for some specific reaction, and optics.¹⁰

Moreover, in the past decade, the research on the structure and chemical bond theory of Ln-MOFs has been at its liveliness, which led to a great deal of new research branches, such as catalysts, monomolecular magnets, magnetic refrigeration materials, and fluorescence recognition.¹¹ So far, the documented Ln-MOFs exhibit that the coordination modes of Ln³⁺ could vary in a wide range with the largest coordination number of 12 due to the various orbital hybridization of fⁿd^{2+m}sp³ (n = 0–3, m = 1–3) devoted by electron orbitals of 6s, 6p, 5d, and 4f, which lead to a series of characteristics in accordance with the intrinsic structures.¹² Thus, although Ln³⁺ ions included in documented Ln-MOFs display the octa- or nano-coordinated modes, they could still possess the strong Lewis acidity and show strong affinities to small guest molecules with smaller steric resistance, such as CO₂, SO₂, N_xO_y, and H₂S. Recently, the metal-organic framework of [Eu(BTB)(phen)] reported by Zhao and coworkers, as the first sample of Ln-MOFs for the fixation of CO₂, display the excellent catalytic behaviour for the chemical transformation of epoxides and CO₂ and into carbonates under mild conditions, which further confirm that the stable octa- or nano-coordinated state of Ln³⁺ ions could be viewed as the strong Lewis acid to polarize and activate the approaching guest molecules.¹³ Whereas, the catalytic performance based on the exposed heterometallic SBUs combined from Ln³⁺ and Zn²⁺ as Lewis acidic sites is unexplored so far.

Thus, based on the above mentioned discussion, our group aimed to synthesize one heterometallic metal-organic framework composed of exposed active Eu³⁺ and Zn²⁺ ions as strong Lewis acidic sites. Meantime, for the anticipated applicability in the aspects of sorption and catalysis, the targeted porous material should possess the basic intrinsic characteristics of thermal stability, solvent-free porosity, and high specific surface area. During the consequent experimental process, a series of common organic ligands were tried under the solvothermal conditions with the adjustment of pH, temperature, the proportion of mixed solvent. Fortunately, the acidic solvothermal reaction of ZnO, Eu₂O₃, and 4,4',4''-(pyridine-2,4,6-triyl)tri(1,3-benzenedicarboxylic acid) (H₆PTTBA) in mixed solvent of DMF/H₂O generated one anticipated robust double-walled honeycomb material of {[Eu^{III}Zn^{II}(HPTTBA)(H₂O)]·4DMF·3H₂O}_n (simplified as NUC-9), in which channels were shaped by undocumented [Eu^{III}Zn^{II}(CO₂)₆(H₂O)] SBUs and conjugated four aromatic rings as the wall. Moreover, NUC-9 could selectively adsorb CO₂ and effectively catalyze the chemical transformation of various epoxides into the related carbonates under comparatively mild conditions. In addition, the fluorescence sensing experiments exhibited that NUC-9 could selectively and sensitively discriminate Fe³⁺ in aqueous solution.

Experimental Section

Materials and General Methods

All chemical reagents were commercially obtained from Jinan Henghua Sci. & Tec. Co. Ltd. without any further refinement. The infrared spectrum (IR) in the range of 500–4000 cm⁻¹ was measured on Nicolet 740 FTIR spectrometer. The element analysis (C, H, and N) was fulfilled on the EA 1110

element analyzer of CE instrument. The powder X-ray diffraction was collected for 2θ values on X-Pert pro diffractometer with Cu-Kα radiation. Thermogravimetric analyses (TGA) were performed on NETZSCH STA 449 F3 thermogravimetric analyzer (25–800°C, 10°C/min, air condition). Single-component gas sorption measurements were performed with an ASAP 2020 Plus instrument: N₂ gas sorption isotherms were measured at 77K using liquid N₂ bath; CO₂ gas sorption isotherms were measured at 273K using ice-water bath and 298K using water bath. The catalytic yield was calculated and measured on a Thermo Fisher Trace ISQ GC/MS instrument. ¹H NMR and ¹³C NMR spectra were recorded on a JEOL-ECX 500 FT (500 and 125 MHz respectively) instrument in CDCl₃ or in DMSO-d₆ with n-dodecane as the internal standard as the internal standard. ICP measurements were performed by a (thermofisher) iCAP Qc ICP-MS emission spectrometer.

Preparation of NUC-9

A mixture of ZnO (0.008 g, 0.1 mmol), Eu₂O₃ (0.018 g, 0.05 mmol), and H₆PTTBA (0.057 g, 0.1 mmol) in mixed solvent of 6 mL DMF and 1 mL H₂O was acidified by HNO₃ (0.2 mL, 0.25 mol/L) and heated in 25 mL autoclave at 110 °C for 4 days and then gradually cooled to room temperature at a rate of 10 °C/h. Colourless crystals of NUC-9 were collected by filtration and washed by DMF/H₂O (3:1). (Yield: 75 % based on H₆PTTBA). Anal. Calcd. for NUC-9 (C₄₁H₄₈ZnN₅O₂₀Eu): C, 42.89; H, 4.18; N, 6.10 (%). Found: C, 42.54; H, 4.42; N, 6.14 (%). IR (KBr pellet, cm⁻¹): 3406 (vs), 1595 (vs), 1394 (vs), 1113 (w), 1018 (w), 783 (s), 705 (w), 514 (w).

X-ray crystallography

The diffraction intensity data for NUC-9 was obtained at 296(2) K by using a Bruker Smart-APEX II CCD area detector (Mo-Kα radiation, λ = 0.071073 nm) with graphite-monochromated radiation. The reflection data were consequently corrected for empirical absorption corrections and Lorentz and polarization effects. The structure was solved by direct methods and refined by full-matrix least-squares with the SHELXL package. All non-hydrogen atoms were refined anisotropically. Hydrogen atoms except those on water molecules were generated geometrically with fixed isotropic thermal parameters, and included in the structure factor calculations. The block of SQUEEZE in PLATON was employed to eliminate the highly disordered solvent molecular. The solvent content of NUC-9 was determined by the thermogravimetric analysis (Fig. S1) and elemental analysis. Crystallographic data and refinement parameter for NUC-9 were listed in Table S1. Selected bond lengths and angles for NUC-9 were concluded in Table S2. Further details on the crystal structure investigations may be obtained from the Cambridge Crystallographic Data Centre, with the depository number CCDC-2002682 for NUC-9.

Catalytic Experiment Operation

Prior to the catalytic coupling reaction, the sample of NUC-9 was immersed in acetone for 24 hours and then dried in vacuum at 120 °C for 12 hours to form the activated catalyst. During the catalytic process, alkyl epoxides were sealed in 20 mL around-bottom flask reactor, which was equipped with magnetic stirrer and heated in temperature-controlled oil bath under ambient pressure. CO₂ was slowly purged into the reactor until the reaction was over. Finally, the product was extracted

with chloroform and the solid catalyst could be easily collected by filtration. The obtained product was analysed by GC and ^1H NMR spectroscopy.

Result and discussion

Crystal structure analysis

Single-crystal X-ray analysis exhibited that **NUC-9** crystallized in a rhombohedral system with $R\bar{3}m$ space group and possess one high-robust double-walled honeycomb host framework with 60.2 % porosity, derived from PLATON calculation. In **NUC-9**, each six rows of $[\text{Eu}^{\text{III}}\text{Zn}^{\text{II}}(\text{CO}_2)_6(\text{H}_2\text{O})]$ SBUs and half equal amount of HPTTBA $^{5-}$ carbon skeletons are alternately arranged to form two classes of tubular nanochannels along the crystallographic axis of c , both of which could be differentiated according to the discrepant inner surface functionalized by free carboxyl oxygen atoms or coordinated aqueous molecules on Eu^{3+} ion. Moreover, except for the excellent characteristics of dual tubular nanochannels, high porosity, and larger specific surface area, the host framework of **NUC-9** contains high density of exposed active metal sites including tetra-coordinated Zn^{2+} cations and octa-coordinated Eu^{3+} cations, which are spanned together by three deprotonated carboxyl groups to form $[\text{Eu}^{\text{III}}\text{Zn}^{\text{II}}(\text{CO}_2)_6(\text{H}_2\text{O})]$ SBUs as Lewis acidic bases, consequently realizing the functionalization of the targeted MOFs. These embodied prominent merits render **NUC-9** to be one potential multifunctional material in current hot research fields of gas separation and storage, organic reaction catalysis, fluorescence recognition, etc. Moreover, it is meaningful that the structural construction mode combined from $[\text{Eu}^{\text{III}}\text{Zn}^{\text{II}}(\text{CO}_2)_6(\text{H}_2\text{O})]$ SBUs and conjugated four aromatic rings of HPTTBA $^{5-}$ as the wall of channels is relatively simple and the host framework is quietly stable up to 390 °C. Meantime, the yield of **NUC-9** by the solvothermal reaction of ZnO , Eu_2O_3 , and H_6PTTBA at 110 °C could reach 95 %, implying the feasibility of industrial production.

As one of highlights, the ligand-directed synthetic strategy could be confirmed by the micro connection fashion between metal ions and HPTTBA $^{5-}$ in **NUC-9**. Under the acidic solvothermal condition with the equal amount of Eu^{3+} and Zn^{2+} , rare earth cation of Eu^{3+} was preferentially coordinated *via* the chelation mode by two deprotonated α -carboxyl groups, shown in Fig. 1b. Based on the basic knowledge of orbital binding energy and our speculation, the reason for the priority coordination right of Eu^{3+} ions is that the binding energies ΔE_n between 4f rare earth cations and coordinated oxygen atoms is larger than the one of 3d transitional metal cations.¹⁴ Of course, in the absence of Eu^{3+} ions, such two deprotonated α -carboxyl groups also could chelate Zn^{2+} ion to lead to one kind of Zn-MOFs with the relatively lower porosity of *ca.* 40 %. Furthermore, it is worth mentioning that only these two α -carboxyl groups nearest to the N atom could synergistically chelate one Eu^{3+} ion, which should be attributed to that the positive charge environment devoted by the protonated hydrogen atom on N atom affect the arrangement of nearest carboxyl groups in one HPTTBA $^{5-}$ ligand from our speculation. Moreover, one $\text{Eu}(\text{CO}_2)_2$ ion and one Zn^{2+} are further spanned together by three different γ -carboxyl groups from three other HPTTBA $^{5-}$ ligands to generate the basic SBUs of $[\text{Eu}^{\text{III}}\text{Zn}^{\text{II}}(\text{CO}_2)_6(\text{H}_2\text{O})]$, in which the Eu^{3+} ion is further

coordinated by one aqueous molecule and Zn^{2+} is linked by the α -carboxyl group furthest from nitrogen atom from another one HPTTBA $^{5-}$ (Fig. 1a and 1b). Totally, the formation of one $[\text{Eu}^{\text{III}}\text{Zn}^{\text{II}}(\text{CO}_2)_6(\text{H}_2\text{O})]$ SBU involves six carboxyl groups offered by five HPTTBA $^{5-}$ ligands. Meantime, six deprotonated carboxyl groups in one HPTTBA $^{5-}$ possess three types of coordination modes: $\mu_1\text{-}\eta^1\text{:}\eta^1$, $\mu_1\text{-}\eta^1\text{:}\eta^0$, and $\mu_2\text{-}\eta^1\text{:}\eta^1$.

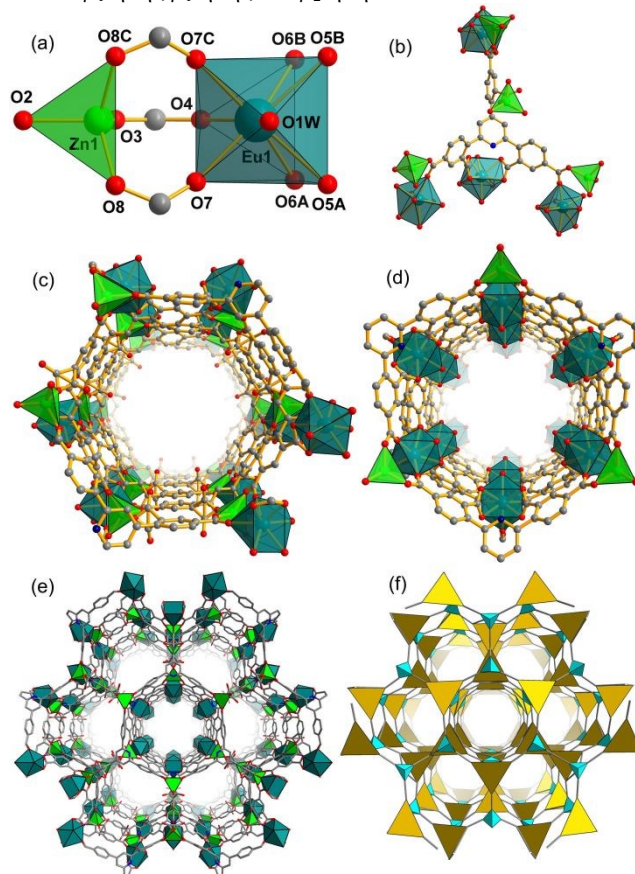


Fig. 1 (a) The $[\text{Eu}^{\text{III}}\text{Zn}^{\text{II}}(\text{CO}_2)_6(\text{H}_2\text{O})]$ heterometallic cluster of **NUC-9**; (b) Coordination mode of HPTTBA ligand; (c) The structural details of channel I; (d) The structural details of channel II; (e) 3D dual-channel framework of **NUC-9**; (f) 3D (5,5)-c fng topology structure with the Schläfli symbol of $\{4^6.6^4\}$ (yellow triangle = HPTTBA ligand and blue polyhedron = heterometallic cluster)(c);

Moreover, as shown in Fig. 1e, $[\text{Eu}^{\text{III}}\text{Zn}^{\text{II}}(\text{CO}_2)_6(\text{H}_2\text{O})]$ SBUs are extended into one double-walled honeycomb structure, which characterized two types of nano-channels (Fig. 1c for **I** and Fig. 1d for **II**) with slightly different aperture of 11.8 Å and 12.6 Å, respectively. Channel **I** exhibits that the only free carboxyl oxygen atoms in each HPTTBA $^{5-}$ stand on the surface of these channel inner wall, which could enhance the polarity of the nano-channel wall and consequently promote the absorption of carbon dioxide.^{15a} Whereas, as shown in Fig. 1d, the associated water molecules on Eu^{3+} cations characterize channel **II** by perpendicularly pointing to the centre of the nano-channel. Thus, channels of **I** and **II** own the completely different functionalized inner surface except for similar exposed metal sites and C-H organic panel on the wall. Finally, for the purpose of visual clarity, the host framework of **NUC-9** could be simplified as a 3D (5,5)-c fng topology with the Schläfli symbol of $\{4^6.6^4\}$ by

reducing $[\text{Eu}^{\text{III}}\text{Zn}^{\text{II}}(\text{CO}_2)_6(\text{H}_2\text{O})]$ SBUs and HPTTBA⁵⁻ ligands as 5-connected nodes, shown in Fig. 1f.

In addition, it is worth mentioning that

with the aid of the designed functionalized hexacarboxyl ligand of H₆TDP (Scheme 1), which possesses several unique characters: (i) Six carboxyl groups may be completely or partially deprotonated to devote rich coordination modes and sequentially build highlight skeletons with nanoporous channels or cages. (ii) The nitrogen atom of pyridine could be protonated and acts as charge balancer, which could effectively tolerate the generation of special skeleton. (iii) The twist angle between central pyridyl planar and three propagated phenyl rings at 2, 4, and 6-position in H₆TDP can be adjusted by itself for adaptive structure self-assembly.

Compared to recently documented neutral framework of $[\text{Eu}(\text{BTB})(\text{phen})]^{13\text{b}}$ and anion of $[\text{Zn}_2(\text{L})(\text{H}_2\text{O})\text{PO}_4]^{15\text{b}}$, **NUC-9** not only consists of these similar exposed metal ions of octa-coordinated Eu³⁺ and tetra-coordinated Zn²⁺, but also features 1D nano-channels and the higher porosity (60.2 % for **NUC-9**, 42.5 % for $[\text{Zn}_2(\text{L})(\text{H}_2\text{O})\text{PO}_4]$, and 56.1 % for $[\text{Eu}(\text{BTB})(\text{phen})]$), which implies that **NUC-9** can more effectively catalyze the chemical transformation of epoxides and CO₂ into related carbonates, especially for the ones with larger substituents. Moreover, it is worth making a brief discussion that these structural characteristics of **NUC-9** could provide one productive self-assembly route for achieving anticipated multifunctional MOFs with nano-tubular channels. Firstly, the employment of ligands is more conducive because the triangle plane of carbon skeleton with a certain degree of twist could be shared by three nano-tubular channels, such as reported MOFs derived from 1,3,5-benzenetricarboxylic acid and 1,3,5-(4-carboxylphenyl)benzene.^{16a} Secondly, in order to enhance the heat and water resistance stability, as many coordination groups as possible participate in coordination without affecting the porosity and the amount of exposed active metal sites, such as employed H₆PTTBA, which combines several unique characters: (i) Six carboxyl groups may be completely or partially deprotonated to devote rich coordination modes and sequentially build highlight skeletons with nanoporous channels or cages. (ii) The nitrogen atom of pyridine could be protonated and acts as charge balancer, which could effectively tolerate the generation of special skeleton. (iii) The twist angle between central pyridyl planar and three propagated phenyl rings at 2, 4, and 6-position in H₆TDP can be adjusted by itself for adaptive structure self-assembly. Thirdly, the usage of DMF or DEF as reaction solvent could effectively avoid the formation of inter-crosslinked structures, may be due to the "template effect".^{16b}

Thermal stability and water stability

Thermogravimetric analysis (TGA) revealed that an initial weight loss of 4.9 % was observed between 70 and 110 °C, corresponding to the removal of lattice water molecules (Fig. S1). In the interval of 220–300 °C, 25.3 % weight loss was observed and in accordance with the elimination of DMF solvent. With temperature rising, the host framework of **NUC-9** could remain stable to 390 °C, indicating its extremely thermal stability. Meanwhile, the PXRD pattern demonstrated that there was no structural collapse after soaking in water at room temperature for

a few days or soaking in boiling water for 48 h (Fig. S2). Thus, the extremely high thermal and water stability of **NUC-9** should be ascribed to the intrinsic strong coordination affinity between $[\text{Eu}^{\text{III}}\text{Zn}^{\text{II}}(\text{CO}_2)_6(\text{H}_2\text{O})]$ SBUs and conjugated four aromatic rings of HPTTBA⁵⁻.

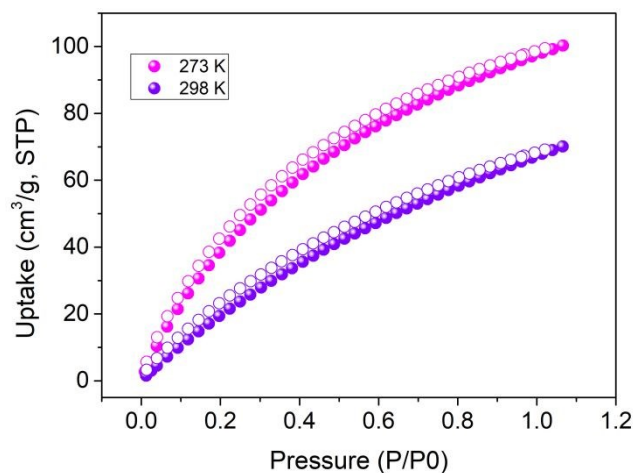


Fig. 2 CO₂ sorption isotherm of **NUC-9** at 273 and 298 K.

Gas Adsorption Studies

For achieving the permanent porosity, the as-synthesized crystalline sample of **NUC-9** was activated by soaking in methanol for three times within one week and consequently vacuum dried at 120 °C for one overnight. The integrity of activated **NUC-9** was confirmed by the PXRD patterns, which was in accordance with the one simulated from X-ray single-crystal diffraction data, shown in Fig. S2. The adsorption performance for N₂ at 77 K exhibited that the total pore volume and the calculated BET surface of activated **NUC-9** were 0.52 cm³/g and 1591 m²/g, respectively. Moreover, the adsorption-desorption isotherm of N₂ displayed a typical type-I sorption configuration and a very sharp uptake at P/P0 < 0.01, representative of microporous material with permanent microporosity, shown in Fig. S3. In addition, analysis of the N₂ adsorption data using the nonlocal density functional theory (NLDFIT) model confirms an aperture distribution in the range of 1.1–1.3 nm, which agreed with the SCXRD analysis, shown in Fig. S3.

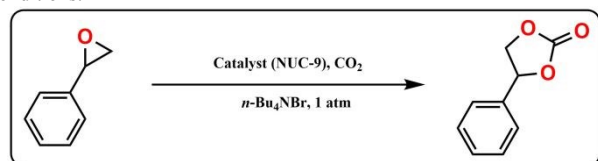
Due to that the innate structural advantages of tubular nanochannels and high density of exposed active metal sites endowed **NUC-9** with the potentiality of adsorbing guest molecules with a quadrupole moment; the affinity for CO₂ was explored at 273 K and 298 K. As shown in Fig. 2, the maximum uptake of CO₂ were 91.07 cm³/g at 273 K and 60.88 cm³/g at 298 K, and meantime the obvious hysteresis loop resulted from the sorption isotherm and incomplete desorption of CO₂ confirmed these strong host-guest interactions. Furthermore, in order to quantify the binding force between CO₂ molecules and the framework of **NUC-9**, the Q_{st} was calculated by the virial method with the resulted value at zero coverage being 25.8 kJ·mol⁻¹, implying that the adsorbed guest molecules of CO₂ could be easily liberated and the host framework of **NUC-9** could be regenerated, shown in Fig. S4.

Catalytic Chemical Reaction of Epoxides with CO₂

The precondition for emerged MOFs to be one effective heterogeneous catalyst on the chemical conversion of CO₂ into

cyclic carbonates is that it could strongly polarize and activate the substrates of epoxides and CO₂ molecules by exposed active metal cations embodied in the host metal-organic framework as strong Lewis acid and weak Lewis base.

Table 1. Cycloaddition Reaction of CO₂ with styrene oxide under various conditions.^a



Entry	NUC-9 (mg)	<i>n</i> -Bu ₄ NBr (mol %)	T (°C)	Yield (%) ^b
1	50	2.5	60	43
2	50	2.5	70	61
3	50	2.5	80	76
4	50	5	60	78
5	50	5	70	99
6	0	5	80	38
7	50	0	80	9

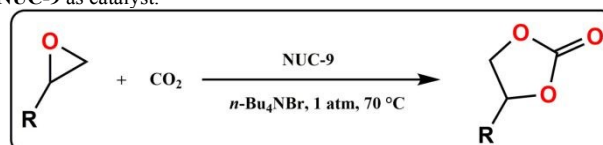
^a Reaction conditions: 20 mmol styrene oxide, 50 mg NUC-9 catalyst, solvent free, CO₂ (1 atm), 8 h. ^b Checked by ¹H NMR and GC-MS spectroscopy with *n*-dodecane as the internal standard.

Impelled by advantage of solvent-free tubular nanochannels, tangible open active sites of Eu³⁺ and Zn²⁺, and free carboxyl oxygen atoms, the catalytic efficiency of activated NUC-9 sample was evaluated by the cycloaddition reaction of epoxides with CO₂ in presence of the classical co-catalyst of tetrabutylammonium (*n*-Bu₄NBr), from which liberated anions of Br could render the substrate of epoxides to form the intermediate of alkyl carbonate anion by the nucleophilic attack. In order to determine the most available temperature, co-catalyst dosage of *n*-Bu₄NBr, and reaction time, the classical solvent-free conditions with 50 mg NUC-9 and 1 atm CO₂ were taken as the benchmark for the transformation reaction of styrene oxide into phenylethylene carbonate, by which the obtained various experimental data was concluded in Table 1. The results of entries 1-3 exhibited that the yield could be increased to 76% with the temperature rising 80 °C for 8 hours, suggesting that the reaction temperature had a crucial effect on the total reaction efficiency. Furthermore, when the quantity of the cheap co-catalyst *n*-Bu₄NBr was doubled, the yield could reach 99% at 70 °C for 8 hours. In order to test the synergetic catalysis, the experiments catalyzed by single NUC-9 or *n*-Bu₄NBr were fulfilled and the results for the yield were unsatisfactory (entries of 6 and 7), which proved that the active open metal sites in NUC-9 and anions of Br possessed the different catalytic advantages for the double-step cycloaddition reaction of epoxides with CO₂. Therefore, the optimal solvent-free reaction conditions of 50 mg (3 mol %) NUC-9 catalyst, 5% mol *n*-Bu₄NBr co-catalyst, and 1 atm CO₂ at 70 °C for 8 hours were used for the subsequent experiments.

In order to verify the universal catalytic applicability of NUC-9 for the chemical fixation of CO₂, a series of representative epoxides with different substituent and steric hindrance under the optimized reaction conditions were fulfilled, listed in Table 2. The obtained results intuitively exhibited that activated NUC-9 displayed the excellent catalytic activity for the substrates of 2-methyloxirane, 2-ethyloxirane, 2-chloro-oxirane,

2-(chloromethyl)oxirane, and 2-phenyloxirane with the yield over 95%. More or less, entry of 6 could demonstrate that the long alkyl chain of 2-(phenoxymethyl)oxirane had an adverse effect on the catalytic cycloaddition reaction, which should be ascribed to the effect of steric hindrance. In addition, it was worth mentioning that the catalytic performance of NUC-9 on epoxides with large substituents was better than the documented tetra-coordinated Zn-based model of [Zn₂(3-tpom)(L)₂],¹⁸ which should be due to that these larger tubular channels in NUC-9 could allow relatively large molecules to enter and leave freely.

Table 2. Cycloaddition reaction of CO₂ and various epoxides with NUC-9 as catalyst.^a



Entry	Epoxides	Products	Yield (%) ^b	Selectivity (%)
1			99	>99
2			99	>99
3			99	>99
4			97	>99
5			99	>99
6			92	>99

^a Reaction conditions: Substrates (20 mmol), *n*-Bu₄NBr (2.5 mol %), NUC-9 catalyst (50 mg), CO₂ (1 atm), 70 °C, 8 h. ^b Determined by GC/MS with *n*-dodecane as the internal standard.

Prior to the application in industrial production, to test the recoverability for one emerged catalyst is the fundamental link due to that the continuous reduction of catalyst quantity will greatly affect the labour cost of industrial monitoring and operation. Thus, a series of continuous amplification experiments by the usage of 500 mg NUC-9 for the cycloaddition reaction of 200 mmol styrene oxide were carried out at 70 °C for 8 hours, which exhibited that NUC-9 could well maintain the catalytic efficiency for five times, shown in Fig. S5. NUC-9 sample was recycled after five cycles of experiments and purged with methanol and dichloromethane to remove *n*-Bu₄NBr and the adherent substrate, leaving a remaining weight of 485 mg with the loss of 3 %. In addition, the PXRD analysis for the recycled NUC-9 sample exhibited that the characteristic peaks were basically fitted with the unused activated one (Fig. S2), which proved that NUC-9 had the potential to be an alternative catalyst for the chemical fixation of CO₂.

In view of the microstructural characteristics of NUC-9, the tested excellent catalytic performance, and documented relevant ratiocinations,¹⁹ the possible reaction mechanism of synergistic catalysis was suggested, elucidated in Fig. 3. At the beginning, the ring of epoxide was polarized and activated by the

electrophilic metal ions of Zn^{2+} and Eu^{3+} located on the surface of the inner wall of these nano-channels. Meantime, the close anion of Br^- liberated from $n-Bu_4NBr$ launched the nucleophilic attack to the less-hindered β -carbon atom of the polarized epoxide, generating the intermediate of 2-bromoalkoxide weakly hanged on the Lewis-acid metal sites. Subsequently, the instantaneous intermediate of alkylcarbonate salt was formed along with the nucleophilic attack of 2-bromoalkoxide to the carbon atom of close polarized CO_2 molecules. Thus, the tendentious cyclization from 2-bromoalkoxide completed the whole reaction with the liberation of catalysts including **NUC-9** and $n-Bu_4NBr$.

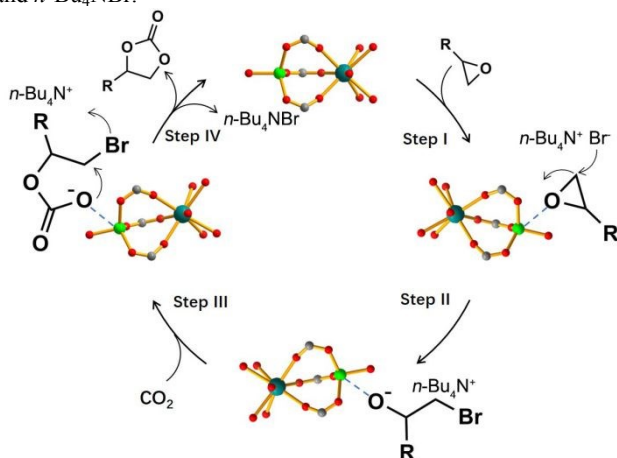


Fig. 3 The catalytic mechanism cycloaddition of epoxides with CO_2 .

Luminescence characteristic and sensing property

The solid-state luminescence spectra of H_6PTTBA ligand and **NUC-9** excited at 320 nm at room temperature were tested and illustrated in Fig. S6. As for H_6PTTBA , the strong emission peak at 450 nm should be ascribed to the intraligand $\pi^* \rightarrow \pi$ electronic transitions among four conjugated aromatic rings. Whereas, for **NUC-9**, five evident characteristic peaks located at 583, 596, 620, 657, and 707 nm in the visible region were in accordance with these ${}^5D_0 \rightarrow {}^7F_J$ ($J = 0, 1, 2, 3,$ and 4) transitions of Eu^{3+} ions, among which the strongest one at 620 nm confirmed that Eu^{3+} ions possessed the asymmetric coordination modes. Moreover, by monitoring the emission at 320 nm, the solid-state PL lifetime of 5D_0 (Eu^{3+}) was determined to be 0.81 ms, shown in Fig. S7. Furthermore, the absolute PL quantum yield (QY) of **NUC-9** with the value of 16.1 % confirmed that organic ligands of $HPTTBA^{5-}$ and $Zn(II)$ cations could synergistically sensitize Eu^{3+} emitters.

In view of uncoordinated carboxyl oxygen atoms and pyridine devoted $HPTTBA^{5-}$ ligand in **NUC-9**, the luminescence sensing experiments were fulfilled towards various metal cations by the followed approaches: equimolar amount of selected 15 typical metal cations was separately dissolved in pre-ultrasonic 3 mL aqueous solution with 2 mg milled sample of **NUC-9** to form $M^{n+}@NUC-9$ ($M = Li^+, Na^+, K^+, Mg^{2+}, Ca^{2+}, Ba^{2+}, Mn^{2+}, Zn^{2+}, Cd^{2+}, Fe^{2+}, Hg^{2+}, Co^{2+}, Ni^{2+}, Cu^{2+}, Al^{3+}, Cr^{3+},$ and Fe^{3+}) aqueous suspension, based on which the luminescence emission intensity at 620 nm were summarized in Fig. 4. Evidently, only the solution introduced with 1.2 mM Fe^{3+} was almost completely luminescence quenched with the efficiency of 98.7%. Consequently, a series of competitive experiments for Fe^{3+} ions with the equimolar amount of other 14 metal cations were carried

out and exhibited that typical common metal ions had no significant effect on the Fe^{3+} -induced luminescence response, which revealed that **NUC-9** could efficiently sense Fe^{3+} ions in water solution without interference (Fig. S8). Moreover, in order to further explore the fluorescence sensitivity of **NUC-9** toward Fe^{3+} ions, luminescence experiments with quantitative titration in the range of 0-1.2 mM were launched, shown in Fig. S9. Meantime, as illustrated in Fig. S10, the gradually reduced fluorescent intensity along with the increased concentration of Fe^{3+} ions was analyzed by the Stern-Volmer (SV) equation of $I_0/I = 1 + K_{sv}[M]$ (K_{sv} : the quenching effect coefficient (M^{-1}), $[M]$: the molar concentration of the metal ions, I_0 and I : the luminescence intensities before and after reaction with metal ions), which displayed that the S-V curve shifted away from the linearity with the concentration of Fe^{3+} ions rising and switched to be well fitted by the equation of $I_0/I = 1.545 \times \exp([Fe^{3+}]/0.044) - 0.667$ ($R^2 = 0.994$). In addition, as shown in Fig. S11, the results by fitting the experimental database of low concentration range of Fe^{3+} shown that **NUC-9** possessed the relatively high K_{sv} value of $4.21 \times 10^4 M^{-1}$, which could be explained by self-absorption or energy-transfer process.²⁰ Moreover, judged by the K_{sv} value and the standard deviation (δ), the detection minimum limit to Fe^{3+} cations could reach 0.1 μM (7.1 ppb) according to the 3 δ IUPAC criteria.

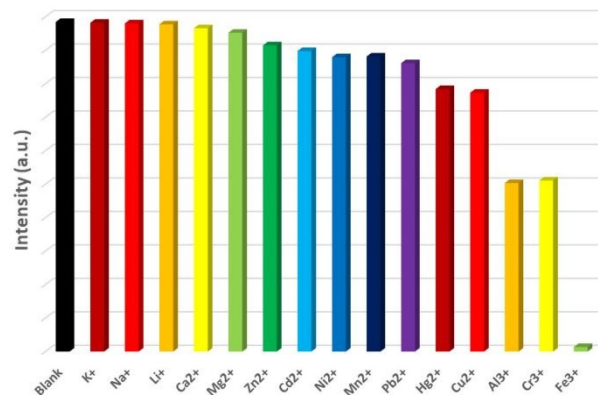


Fig. 4 Emission intensity **NUC-9** aqueous suspensions with different metal ions.

Based on the structural characteristics of **NUC-9** and related documented studies on fluorescence recognition by MOFs,²¹ the possible luminescence sensing mechanism toward Fe^{3+} ions were deduced. Just as shown in Fig. S2, although major peaks of the powder X-ray diffraction on the recycled **NUC-9** could coincide with the ones of the original sample, several emerged weak peaks should be ascribed to the affinity between Fe^{3+} ions and the host framework of **NUC-9**. In addition, the ICP results revealed that no Eu^{3+} ions were detected in the $NUC-9@Eu^{3+}$ suspension after luminescence experiments, implying that the fluorescence quenching was not caused by ion exchange (Table S3). Further UV-visible absorption spectra of Fe^{3+} and the excitation spectra of **NUC-9** displayed a large overlap, indicating that the competitive absorption existed between Fe^{3+} and the framework of **NUC-9** (Fig. S12), generating one $Fe^{3+}@NUC-9$ intermediate in aqueous solution along with a decline of luminescence intensity of Eu^{3+} -based chromophores due to the reduction of energy transfer efficiency from $HPTTBA$ ligands to the Eu^{3+} ion.

Conclusions

By utilizing the ligand-directed synthetic strategy, the solvothermal self-assembly of Zn^{2+} and Eu^{3+} ions with the aid of the pre-designed H_6PTTBA generated one robust double-walled honeycomb material of **NUC-9**, which exhibited the excellent catalytic performance for the chemical transformation of various epoxides into the related carbonates under comparatively mild conditions of 1 atm CO_2 flow and 70 °C. Meantime, the water-resistant framework of **NUC-9** could selectively and sensitively discriminate Fe^{3+} ions in aqueous solution. In fact, **NUC-9** represented one class of emerged heterometallic nanoporous materials based on heterometallic binuclear SBUs. Such materials not only featured the characteristics of dual tubular nanochannels, high porosity and specific surface area, but also possessed tetra-coordinated transition metal ions and octa-coordinated rare earth ions. Although ions of Zn^{2+} and Eu^{3+} were selected to construct the targeted model for the catalytic study on the chemical fixation of CO_2 by our group, other combinations from any transition metal ions and octa-coordinated rare earth ions with the aid of H_6PTTBA also could be assembled for other specific functional researches in the future, such as optics, magnetism, and so on.

Conflicts of interest

The authors have no conflicts of interest to declare.

Acknowledgements

The work was supported by financial support from the Natural Science Foundation of China (21101097, 21801230), the Opening Foundation of Key Laboratory of Laser & Infrared System of Shandong University (2019-LISKFJJ-005), and the start-up funds of North University of China.

References

- a) S. A. Montzka, E. J. Dlugokencky, J. H. Butler, *Nature*, **2011**, 476, 43; b) J. D. Shakun, P. U. Clark, F. He, S. A. Marcott, A. C. Mix, Z. Y. Liu, B. Otto-Bliessner, A. Schmittner, E. Bard, *Nature*, **2012**, 484, 49; c) P. Lanzafame, G. Centi, S. Perathoner, *Chem. Soc. Rev.*, **2014**, 43, 7562; d) Y. Wang, J. Ding, Y. Wang, X. Zhou, Y. Cao, B. Ma, J. Li, X. Wang, T. Seto, Z. Zhao, *J. Mater. Chem. C*, **2019**, 7, 1792; e) T. Yuan, T. Meng, P. He, Y. Shi, Y. Li, X. Li, L. Fan, S. Yang, *J. Mater. Chem. C*, **2019**, 7, 6820; f) V. Amoli, S. Y. Kim, J. S. Kim, H. Choi, J. Koo, D. H. Kim, *J. Mater. Chem. C*, **2019**, 7, 14816; g) S. Zhao, R. Jin, *ACS energy Lett*, **2018**, 3, 425.
- a) A. Goepfert, M. Czaun, G. K. Surya Prakash, G. A. Olah, *Energy Environ. Sci.*, **2012**, 5, 7833; b) H. Wang, Z. Zhang, H. Wang, L. Guo, L. Li, *Dalton Trans.* **2019**, 48, 15970; c) E. S. Sanz-Pérez, C. R. Murdock, S. A. Didas, C. W. Jones, *Chem. Rev.*, **2016**, 116, 11840; d) M. Z. Jacobson, *Energy Environ. Sci.*, **2009**, 2, 148; e) D. M. Fernandes, A. F. Peixoto, C. Freire, *Dalton Trans.* **2019**, 48, 13508.
- a) C. Li, X. Tong, P. Yu, W. Du, J. Wu, H. Rao, Z. M. Wang, *J. Mater. Chem. A*, **2019**, 7, 16622; b) Y. Wu, X. Song, S. Xu, Y. Chen, O. Oderinde, L. Gao, R. Wei, G. Xiao, *Dalton Trans.* **2020**, 49, 312.; c) J. Zhu, J. Liu, Y. Machain, B. Bonnett, S. Lin, M. Cai, M. C. Kessinger, P. M. Usov, W. Xu, S. D. Senanayake, D. Troya, A. R. Esker, A. J. Morris, *J. Mater. Chem. A*, **2018**, 6, 22195; d) M. Wang, W. Zhong, S. Zhang, R. Liu, J. Xing, G. Zhang, *J. Mater. Chem. A*, **2018**, 6, 9915; e) D. Ma, B. Li, K. Liu, X. Zhang, W. Zou, Y. Yang, G. Li, Z. Shi, S. Feng, *J. Mater. Chem. A*, **2015**, 3, 23136.
- a) S. Wang, K. Song, C. Zhang, Y. Shu, T. Li, B. Tan, *J. Mater. Chem. A*, **2017**, 5, 1509; b) F. Guo, X. Zhang, *Dalton Trans.* **2020**, 49, 9935; c) S. Li, L. Zhang, Y. Lan, K. P. O'Halloran, H. Ma, H. Pang, *Nature Comm.*, **2020**, 11, 497; d) S. Luo, Z. Zeng, G. Zeng, Z. Liu, R. Xiao, P. Xu, H. W., D. Huang, Y. Liu, B. Shao, Q. Liang, D. Wang, Q. He, L. Qin, Y. Fu, *J. Mater. Chem. A*, **2020**, 8, 6434; e) L. Shi, Z. Li, L. Ju, A. Carrasco-Pena, N. Orlovskaya, H. Zhou, Y. Yang, *J. Mater. Chem. A*, **2020**, 8, 1059.
- a) Z. Ma, P. Li, L. Ye, Y. Zhou, F. Su, C. Ding, H. Xie, Y. Bai, P. K. Wong, *J. Mater. Chem. A*, **2017**, 5, 24995; b) S. Luo, X. Li, M. Wang, X. Zhang, W. Gao, S. Su, G. Liu, M. Luo, *J. Mater. Chem. A*, **2020**, 8, 5647; c) L. Sun, Y. Yun, H. Sheng, Y. Du, Y. Ding, P. Wu, P. Li, M. Zhu, *J. Mater. Chem. A*, **2018**, 6, 15371.
- a) Y. Sun, X. Jia, H. Huang, X. Guo, Z. Qiao, C. Zhong, *J. Mater. Chem. A*, **2020**, 8, 3180; b) R. Babu, R. Roshan, Y. Gim, Y. H. Jang, J. F. Kurisingal, D. W. Kim, D.-W. Park, *J. Mater. Chem. A*, **2017**, 5, 15961; c) L. Huang, B. Li, B. Su, Z. Xiong, C. Zhang, Y. Hou, Z. Ding, S. Wang, *J. Mater. Chem. A*, **2020**, 8, 7177; d) X. L. Lv, L. H. Xie, B. Wang, M. Zhao, Y. Cui, J. R. Li, *J. Mater. Chem. C*, **2018**, 6, 10628.
- a) F. Schönfeld, L. V. Meyer, F. Mühlbach, S. H. Zottnick, K. Müller-Buschbaum, *J. Mater. Chem. C*, **2018**, 6, 2588; b) A. Yousaf, A. M. Arif, N. Xu, J. Zhou, C. Y. Sun, X. L. Wang, Z.-M. Su, *J. Mater. Chem. C*, **2019**, 7, 8861; c) H. Li, Q. Li, Z. Xu, *J. Mater. Chem. C*, **2019**, 7, 2880; d) C. Li, W. Yang, X. Zhang, Y. Han, W. Tang, T. Yue, Z. Li, *J. Mater. Chem. C*, **2020**, 8, 2054; e) F. Y. Yi, S. C. Wang, M. Gu, J. Q. Zheng, L. Han, *J. Mater. Chem. C*, **2018**, 6, 2010.
- Y. H. Luo, A. D. Xie, W. C. Chen, D. Shen, D. E. Zhang, Z. W. Tong, C. S. Lee, *J. Mater. Chem. C*, **2019**, 7, 14897.
- a) Y. X. Zhang, B. X. Li, H. Lin, Z. Ma, X. T. Wu, Q. L. Zhu, *J. Mater. Chem. C*, **2019**, 7, 6217; b) J. M. Liu, J. X. Hou, J. Liu, X. Jing, L. J. Li, J. L. Du, *J. Mater. Chem. C*, **2019**, 7, 11851.
- a) A. M. Kaczmarek, P. V. D. Voort, *J. Mater. Chem. C*, **2019**, 7, 8109; b) S. Basu, S. Bhandari, U. N. Pan, A. Paul, A. Chattopadhyay, *J. Mater. Chem. C*, **2018**, 6, 8205.
- a) S. Jensen, K. Tan, W. Lustig, D. Kilin, J. Li, Y. J. Chabal, T. Thonhauser, *J. Mater. Chem. C*, **2019**, 7, 2625; b) E. L. Zhou, C. Qin, D. Tian, X. L. Wang, B. X. Yang, L. Huang, K. Z. Shao, Z. M. Su, *J. Mater. Chem. C*, **2018**, 6, 7874; c) E. Angioni, R. J. Marshall, N. J. Findlay, J. Bruckbauer, B. Breig, D. J. Wallis, R. W. Martin, R. S. Forgan, P. J. Skabara, *J. Mater. Chem. C*, **2019**, 7, 2394; d) Y. Cheng, Y. Gao, H. Lin, F. Huang, Y. Wang, *J. Mater. Chem. C*, **2018**, 6, 7462.
- Y. J. Ma, S. D. Han, J. Pan, Y. Mu, J. H. Li, G. M. Wang, *J. Mater. Chem. C*, **2018**, 6, 9341.
- a) W. P. Lustig, S. J. Teat, J. Li, *J. Mater. Chem. C*, **2019**, 7, 14739; b) H. Xu, B. Zhai, C. S. Cao, B. Zhao, *Inorg. Chem.* **2016**, 55, 9671.
- J. Sun, P. Guo, M. Liu, H. Li, *J. Mater. Chem. C*, **2019**, 7, 8992.
- a) L. Zhai, Z. X. Yang, W. W. Zhang, J. L. Zuo, X. M. Ren, *J. Mater. Chem. C*, **2018**, 6, 7030; b) M. Gupta, D. De, K. Tomar, P. K. Bharadwaj, *Inorg. Chem.* **2017**, 56, 14605.
- a) A. Schoedel, M. Li, D. Li, M. O'Keeffe, O. M. Yaghi, *Chem. Rev.* **2016**, 116, 12466; b) Y. J. Li, Y. L. Wang, Q. Y. Liu, *Inorg. Chem.* **2017**, 56, 2159.
- a) X. P. Wang, W. M. Chen, X. Y. Li, Rajnák. Cyril, D. Sun, *Chem. Eur. J.* **2017**, 23, 7990; b) W. M. Chen, X. L. Meng, G. L. Zhuang, Z. Wang, M. Kurmoo, Q. Q. Zhao, X. P. Wang, B. Shan, C. H. Tung, D. Sun, *J. Mater. Chem. A*, **2017**, 5, 13079; c) D. Sun, G. G. Luo, N. Zhang, J. H. Chen, R. B. Huang, L. R. Lin, L. S. Zheng, *polyhedron*, **2009**, 28, 2983; d) D. Sun, Z. H. Yan, M. Liu, H. Xie, S. Yuan, H. Lu, S. Feng, D. Sun, *Cryst. Growth Des.* **2012**, 12, 2902; e) L. L. Han, T. P. Hu, K. Mei, Z. M. Guo, C. Yin, Y. X. Wang, J. Zheng, X. P. Wang, D. Sun, *Dalton Trans.* **2015**, 44, 6052.
- V. Gupta, S. K. Mandal, *Inorg. Chem.* **2020**, 59, 4273.
- a) Z. F. Wu, E. Velasco, C. Shan, K. Tan, Z. Z. Zhang, Q.-Q. Hu, K. Xing, X. Y. Huang, J. Li, *J. Mater. Chem. C*, **2020**, <https://doi.org/10.1039/D0TC00825G>; b) D. Jiang, X. Yang, X. Zheng, L. Bo, T. Zhu, H. Chen, L. Zhang, S. Huang, *J. Mater. Chem. C*, **2018**, 6, 8513.
- a) B. C. Tzen, J. F. Lin, *Dalton Trans.* **2020**, <https://doi.org/10.1039/C8DT04904A>; b) D. Xu, L. Chen, X. Dai, B. Li, Y. Wang, W. Liu, J. Li, Y. Tao, Y. Wang, Y. Liu, G. Peng, R. Zhou, Z. Chai, S. Wang, *ACS Sustainable Chem. Eng.* **2020**, 12, 15288; c) W. Chi,

- J. Chen, W. Liu, C. Wang, Q. Qi, Q. Qiao, T. M. Tan, K. Xiong, X. Liu, K. Kang, Y. T. Chang, Z. Xu, X. Liu, *J. Am. Chem. Soc.* **2020**, *142*, 6777; d) C. Y. Liu, X. R. Chen, H. X. Chen, Z. Niu, H. Hirao, P. Braunstein, J.-P. Lang, *J. Am. Chem. Soc.* **2020**, *142*, 6690; e) T. Y. Li, D. S. M. Ravinson, R. Haiges, P. I. Djurovich, M. E. Thompson, *J. Am. Chem. Soc.* **2020**, *142*, 6158; f) B. Liu, M. Böckmann, W. Jiang, N. L. Doltsinis, Z. Wang, *J. Am. Chem. Soc.* **2020**, *142*, 7092; g) X. Hei, W. Liu, K. Zhu, S. J. Teat, S. Jensen, M. Li, D. M. O'Carroll, K. Wei, K. Tan, M. Cotlet, T. Thonhauser, J. Li, *J. Am. Chem. Soc.* **2020**, *142*, 4242.
21. a) X. Hu, L. Zhong, C. Shu, Z. Fang, M. Yang, J. Li, D. Yu, *J. Am. Chem. Soc.* **2020**, *142*, 4621; b) X. Wu, D. G. Chen, D. Liu, S. H. Liu, S. W. Shen, C. I. Wu, G. Xie, J. Zhou, Z. X. Huang, C. Y. Huang, S. J. Su, W. Zhu, P. T. Chou, *J. Am. Chem. Soc.* **2020**, *142*, 7469; c) Y. X. Hu, X. Hao, L. Xu, X. Xie, B. Xiong, Z. Hu, H. Sun, G. Q. Yin, X. Li, H. Peng, H.-B. Yang, *J. Am. Chem. Soc.* **2020**, *142*, 6285; d) Y. L. Wang, C. Li, H. Q. Qu, C. Fan, P. J. Zhao, R. Tian, M. Q. Zhu, *J. Am. Chem. Soc.* **2020**, *142*, 7497; e) Yang, O. Jacobson, F. Zhang, P. Huang, X. Chen, *J. Am. Chem. Soc.* **2020**, *142*, 6822; f) S. Yuan, L. Huang, Z. Huang, D. Sun, J. S. Qin, L. Feng, J. Li, X. Zou, T. Cagin, H. C. Zhou, *J. Am. Chem. Soc.* **2020**, *142*, 4732.

Graphical Abstract

One robust double-walled honeycomb material of $\{[Eu^{III}Zn^{II}(HPTTBA)(H_2O)] \cdot 4DMF \cdot 3H_2O\}_n$ with excellent catalytic performance on the chemical fixation of CO_2 was presented by utilizing the ligand-directed synthetic strategy.

